Dalton Transactions

ROYAL SOCIETY OF CHEMISTRY

PAPER

View Article Online
View Journal | View Issue

Cite this: *Dalton Trans.*, 2026, **55**, 635

Oxidative dehydrogenation of C_2H_6 and CO_2 mediated by $Rh_xNb_y^-$ ($x + y = 5$) clusters

Hai Zhu, Xin-Yue Sun and Xiao-Na Li *

Received 29th October 2025,
Accepted 2nd December 2025

DOI: 10.1039/d5dt02594j

rsc.li/dalton

Oxidative dehydrogenation (ODHE) of C_2H_6 and CO_2 to generate C_2H_4 and CO is industrially important but remains a long-standing challenge due to the complexity of this co-conversion and the thermodynamically stable and kinetically inert nature of both reactants. Herein, we theoretically demonstrated that the $Rh_xNb_y^-$ ($x + y = 5$) bimetallic clusters can drive the ODHE of C_2H_6 and CO_2 to produce C_2H_4, CO, and H_2O. The results indicated that the desorption of C_2H_4 and CO takes place under mild conditions, and the increased number of Rh atoms in $Rh_xNb_y^-$ leads to progressively more difficult C_2H_4 desorption. In contrast, the formation and evaporation of H_2O represent the kinetically and thermodynamically demanding pathway to govern the overall efficiency of ODHE. This finding provides an integrated picture to understand the fundamental mechanisms of the ODHE of C_2H_6 and CO_2. The selective release of C_2H_4 and the rate-determining behaviour of H_2O generation were rationalized.

Introduction

Carbon dioxide (CO_2) represents the most significant greenhouse gas in the Earth's atmosphere, surpassing methane (CH_4) and nitrous oxide and becoming the principal contributor to global warming.[1–3] To reduce CO_2 emissions and mitigate greenhouse effect,[4–6] countries worldwide are actively exploring novel strategies for the resource utilization of CO_2.[7–11] However, the achievement of CO_2 activation and subsequent conversion under mild conditions poses serious challenges owing to the thermodynamic stability and kinetic inertness of the O–CO bond (5.48 eV).[12,13] Nowadays, we are in the midst of the third revolution in the oil and gas industry owing to the emergence of shale gas chemistry.[14–16] The primary components of shale gas are low-carbon alkanes (CH_4 and C_2H_6, ~90%);[15,17–19] in this case, CO_2, serving as an appealing mild oxidant source, can be used in the transformation of light alkanes to synthesize industrial feedstocks and prevent over-oxidation.[20] Meanwhile, C_2H_6, as the second abundant component (3%–12%) after CH_4 in shale gas, is distinctly underutilized. The oxidative dehydrogenation (ODHE) of C_2H_6 and CO_2 ($C_2H_6 + CO_2 \rightarrow C_2H_4 + CO + H_2O$, $\Delta H_0 = +1.86$ eV)[17,21–24] is a promising route to generate C_2H_4, which represents one of the most important intermediates in the chemical industry. Considerable efforts have been made to improve the performance of related heterogeneous catalysts and drive these conversions taking place under mild conditions, such as controlling the ratio of active components,[21] altering the composition of the reactive phase interface,[21,22,25] and modifying the catalyst support.[26,27] The central goal of these strategies lies in engineering the microenvironment of active sites that govern the catalytic conversion. However, it is a big challenge to understand the nature of active sites and get a fundamental understanding of reaction mechanisms due to the inherent complexity of real-life catalysts.[28]

Gas-phase cluster study emerges as a promising approach to face this challenge because the active sites involved in the activation and transformation of reactants in condensed-phase catalysts are typically composed of a limited number of atoms.[29,30] Cluster reactions performed under isolated conditions provide prominent advantages to permeate and modify the geometrical and electronic structures of active species microscopically, thereby providing the scientific guidance to design superior catalysts.[31–35] The unique geometrical and electronic properties of Nb- and Rh-containing clusters endow them with high reactivity in C_2H_6 dehydrogenation or CO_2 reduction. The Luo group demonstrated that the pure Nb_n^+ (n = 1–21) and Rh_n^+ (n = 1–24) clusters can drive C_2H_6 dehydrogenation to generate $Nb_nC_{1-4}^+$ and $Rh_nC_2H_4^+$.[36,37] Ma and He identified that the Nb- and Rh-containing clusters, such as $Nb_3C_4^-$,[38] $Nb_2BN_2^-$,[39] $RhTaC_2^-$,[40] $Rh_2VO_{2-3}^-$,[41] $RhTiO_2^-$,[42] $Rh_nVO_{3,4}^-$ (n = 3–7),[43] and Rh_n^- (n = 3–11),[44] exhibit outstanding reactivity in CO_2 reduction. These studies indicate that the Rh–Nb heteronuclear clusters can be potential candidates to drive the catalytic conversion of C_2H_6 and CO_2; however, such studies have not been reported in the gas phase. Herein, we theoretically designed and demonstrated that a series of $Rh_xNb_y^-$ ($x + y = 5$) clusters can drive the ODHE of C_2H_6 and

Key Laboratory of Cluster Science of Ministry of Education, School of Chemistry and Chemical Engineering, Beijing Institute of Technology, Beijing 102488, P. R. China. E-mail: xiaonali@bit.edu.cn

CO_2. This chosen cluster size represents a computationally tractable model that allows for relatively exhaustive exploration of pathways while being sufficiently large to capture the composition-dependent reactivity of $Rh_xNb_y^-$ in the catalysis of CO_2-assisted dehydrogenation of C_2H_6. Note that theoretical calculations with density functional theory (DFT) have been demonstrated to be powerful enough to predict the structure and properties of a particular kind of catalysts, and some predicted species have been substantiated in experiments.[45,46] These fascinating results are of substantial importance to understand the nature of Rh–Nb-based heterogeneous catalysts in driving the ODHE of C_2H_6 and CO_2 at a strictly molecular level.

Results

The lowest-lying isomers and the electrostatic potential (ESP) maps of the $Rh_xNb_y^-$ ($x + y = 5$) clusters are shown in Fig. 1A, and the other DFT-calculated low-lying isomers of $Rh_xNb_y^-$ are shown in Fig. S1 and S2 in the SI. It is obvious that the number of Rh atoms in $Rh_xNb_y^-$ significantly affects the geometrical and electronic structures of the clusters (Fig. 1A), and the negative charges accumulate gradually towards the periphery of clusters because of the larger electronegativity of Rh than that of Nb (Rh = 2.28, Nb = 1.60).[24] Note that the positively charged environment[47] is more favourable to polarize alkane molecules because the σ (C–H) orbital of alkane generally acts as an electron donor while the empty orbital of clusters behaves as the acceptor. Therefore, clusters surrounded by negatively charged metal atoms can be less accessible for alkane molecules.[48–50] Fig. 1B displays clearly that it is more challenging for the initial approach of C_2H_6 towards $^3RhNb_4^-$, with respect to other $Rh_xNb_y^-$ clusters.

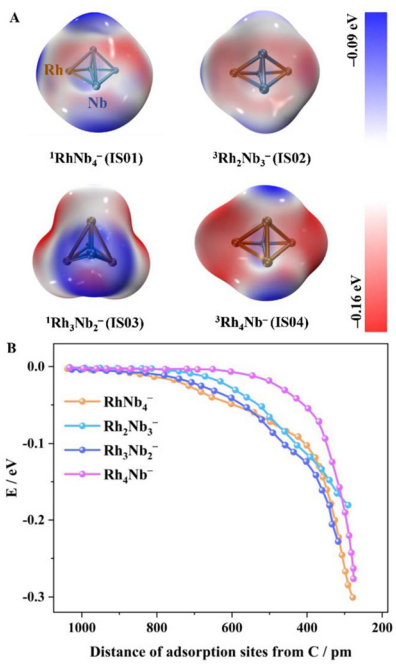

Fig. 1 ESP maps for $^1RhNb_4^-$, $^3Rh_2Nb_3^-$, $^1Rh_3Nb_2^-$, and $^3Rh_4Nb^-$. The superscripts represent spin multiplicities (A). Relaxed potential energy curve with the approach of C_2H_6 towards the $Rh_xNb_y^-$ clusters (B).

The pathways in the reaction of $^1RhNb_4^-$ (IS01) with C_2H_6, as well as the reaction of product $^3RhNb_4H_2^-$ after C_2H_4 evaporation with CO_2, are illustrated in Fig. 2 and 3 to understand the mechanisms of the ODHE of C_2H_6 and CO_2 mediated by $Rh_xNb_y^-$, and other results are presented in Fig. S6–S11. Fig. 2 shows that C_2H_6 prefers to be weakly attached to a single Nb atom (Nb1) (^{1}I1, ΔH_0: −0.28 eV) through two H atoms. Driven by the strong Nb–C (5.43 eV) and Nb–H (2.30 eV) bonds,[12] the first C–H bond of C_2H_6 undergoes oxidative addition through a positive barrier of +0.11 eV (^{1}TS1). The transferred H atom is captured by two nearby Nb atoms, and the resulting intermediate is greatly stabilized (^{1}I2, ΔH_0: −1.31 eV). This step is generally recognized as the rate-limiting step in the initial alkane activation.[51] The subsequent H atom transfer steps occur on a relatively flat pathway (^{1}I2 → ^{3}I3, Fig. 2 and S3) and a spin flip process from the singlet to the triplet state is required. Activation of the second C–H bond from ^{3}I3 is facile to proceed (^{3}TS3: ΔH_0: −1.14 eV) to give rise to a significantly stabilized intermediate ^{3}I4 (ΔH_0: −2.41 eV), which has enough internal energy to evaporate C_2H_4 into the gas phase and produce $^3RhNb_4H_2^-$ ($^3P_1 + C_2H_4$: ΔH_0: −0.49 eV). Moreover, an alternative pathway involving the recombination of two H atoms to generate H_2 is seemingly more favourable ($^1P_2 + H_2$: ΔH_0: −0.62 eV). However, H_2 desorption is entropically disfavoured (ΔG_{298} = −0.38 eV) with respect to C_2H_4 evaporation (ΔG_{298} = −0.52 eV) owing to the intricate and convoluted H migration and H–H coupling steps to drive H_2 generation, reinforcing that C_2H_4 desorption is an entropy-driven process. Moreover, the route to rupture the C–C bond of C_2H_4 from ^{3}I4 to generate CH_4, a competitive product that commonly decreases the selectivity of C_2H_4, was also considered (Fig. S3). The calculations confirm that CH_4 formation is thermodynamically more favorable, but the slightly higher kinetic barrier to form the fourth C–H bond of CH_4 makes CH_4 generation kinetically hindered.

The resulting product, $^3RhNb_4H_2^-$, can capture a CO_2 molecule. Fig. 3 shows that CO_2 can be anchored by two Nb atoms with a large binding energy of 2.53 eV (^{1}I7), during a process in which CO_2 is highly activated with the O–C–O angle changing from 180° in the free state to 135° in ^{1}I7. In the next step, the O–CO bond is ruptured to form a more stable intermediate ^{3}I8 (ΔH_0: −3.14 eV), from which two distinct pathways emerge to close the catalytic cycle. The key difference between the two pathways is whether H_2O generation occurs with (path I) or without (path II) CO attached to the cluster. In path I, the couplings of two O–H bonds (^{1}TS7 and ^{1}TS8) to form the attached H_2O molecule (^{3}I12) represent the rate-determining steps, followed by consecutive desorption of CO and H_2O from the system. Note that these desorption processes are energetically demanding, and elevated temperatures are required. Although yielding the same thermodynamic products, the O–H coupling processes in path II that occur without CO attach-

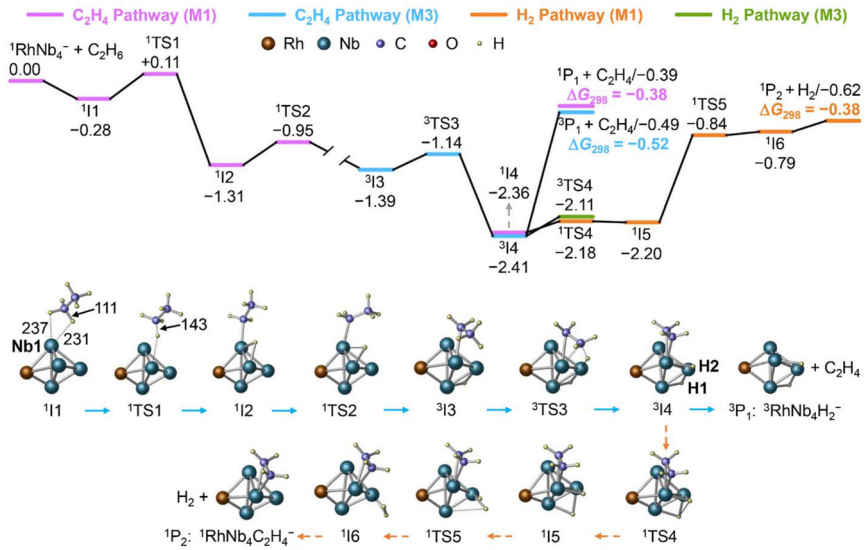

Fig. 2 DFT-calculated potential energy profile for the reaction $^{1}RhNb_4^-$ + C_2H_6. Relative energies (ΔH_0/eV and ΔG_{298}/eV) for intermediates (Is) and transition states (TSs) are shown. The superscripts represent spin multiplicities. Bond lengths are given in pm. See details in Fig. S3.

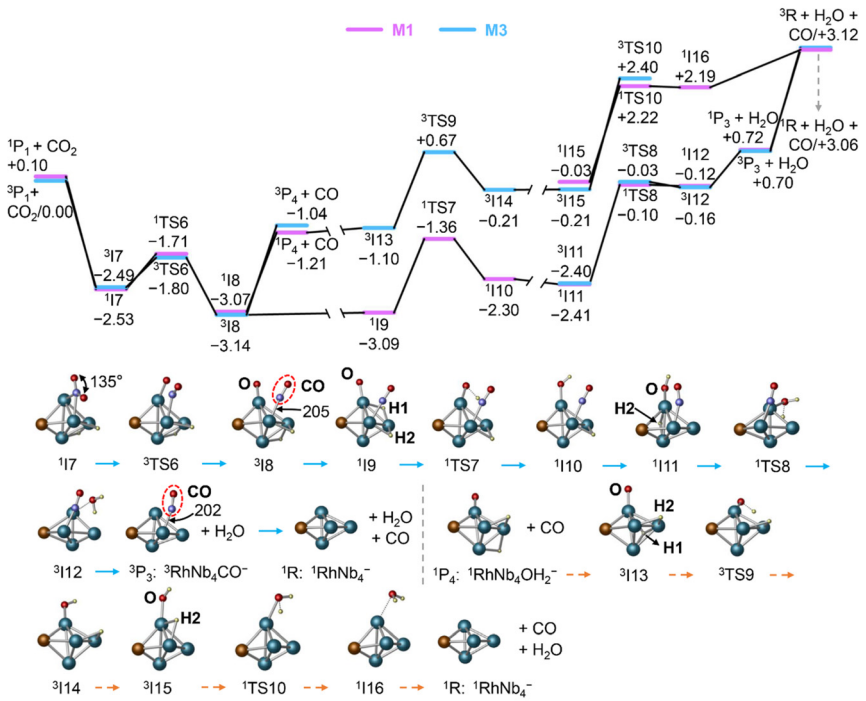

Fig. 3 DFT-calculated potential energy profile for the reaction $^{3}RhNb_4H_2^-$ ($^{3}P_1$) + CO_2. Relative energies (ΔH_0/eV) for Is and TSs are shown. The superscripts represent spin multiplicities. Bond lengths are given in pm. See details in Fig. S4.

ment must overcome substantially higher kinetic barriers (^{3}TS9 and ^{1}TS10). Concurrently, CO could desorb prior to H_2O formation because of the thermodynamically feasible process (ΔH_0: −1.21 eV). A comprehensive survey on this ODHE process of C_2H_6 and CO_2 mediated by $^{1}RhNb_4^-$ highlights that the generation of C_2H_4 and desorption of CO occur under near-ambient conditions (Fig. 2), while the final formation and evaporation of H_2O into the gas phase is thermodynamically and kinetically challenging to limit the overall efficiency of the catalysis (Fig. 3). A similar trend is observed in driving the catalysis of ODHE of C_2H_6 and CO_2 mediated by other $Rh_xNb_y^-$ clusters (Fig. S6–S11), and the increased number of Rh atoms ($x > 1$) in $Rh_xNb_y^-$ makes C_2H_4 generation kinetically or thermodynamically more difficult compared to the pathway mediated by $RhNb_4^-$ (Fig. 2 and S6, S8, S10). In summary, with the increase in Rh atoms in the

$Rh_xNb_y^-$ clusters, the desorption of C_2H_4 or H_2 happens from the Nb site towards the Rh site (Fig. S10). Note that the Rh–C (6.01 eV) and Rh–H (2.50 eV) bonds are stronger than Nb–C (5.43 eV) and Nb–H (2.30 eV) bonds,[12] respectively; therefore, the desorption of both products becomes more challenging. This conclusion parallels extensive experimental observations that Rh can facilitate C–H activation and induce coke deposition at the same time.[52,53] To get a comprehensive understanding of these catalytic reactions mediated by $Rh_xNb_y^-$, the rate-determining steps are summarized in Table 1.

The importance of the order of reactant feed has been identified for the co-conversion of CH_4 and CO_2 in gas-phase experiments; the pre-interaction of metal clusters with CH_4 rather than CO_2 is pivotal for the formation of value-added products.[54–56] Thus, the adsorption of CO_2 prior to C_2H_6 on $^1RhNb_4^-$ was investigated and the calculated results demonstrated that the reduction of CO_2 into gas-phase CO by $^1RhNb_4^-$ is a highly exothermic process to generate the isolated product $^1RhNb_4O^-$ (ΔH_0: −1.06 eV, Fig. S5A), which can also convert C_2H_6 into gas-phase C_2H_4 under relatively mild conditions (Fig. S5B). In marked contrast, the subsequent formation and evaporation of H_2O from the system is a substantially endothermic step (ΔH_0: +3.64 eV) and higher temperatures are indispensable to regenerate the reactant cluster $^1RhNb_4^-$. Note that catalysts cannot regulate the enthalpy of a catalytic reaction; thus, the thermodynamically more favorable step of CO_2 reduction mediated by $^1RhNb_4^-$ reasonably results in a more demanding process of H_2O evaporation. This finding further underscores the significance of introducing reactants in the correct order, as the initial activation of C_2H_6 into gas-phase C_2H_4 on clusters represents an energy-efficient pathway for the ODHE of C_2H_6 and CO_2.

Discussion

Composition-dependent catalytic reactivity of $Rh_xNb_y^-$ ($x + y = 5$) in the ODHE of C_2H_6 by CO_2

In condensed-phase systems, the co-conversion of C_2H_6 and CO_2 exhibits significant complexity due to the competing processes of C–C bond preservation (ODHE of C_2H_6 into C_2H_4) and cleavage (dry reforming of C_2H_6 and CO_2 into synthesis gas).[22,23,57,58] The structural simplicity of supported monometallic catalysts (*e.g.*, Co,[59,60] Ni,[21,23] Ga,[61,62] and Cr[63–65]) faces the challenges to balance the selectivity of this catalytic conversion. In contrast, supported bimetallic catalysts (*e.g.*, NiMo,[23] $PdCo_x$,[66] Ni_1Fe_3,[21] PtNi,[27,57] and PdFe[17]) can effectively mitigate C–C scission and drive dehydrogenation, benefiting from synergistic effects (such as electronic effects, geometric effects, and bifunctional mechanisms). For example, the supported bimetallic catalyst Ni_1Fe_3 [21] can greatly suppress side reactions (*e.g.*, coking from thermal cracking) and enhance the selectivity of C_2H_6 and CO_2 conversion towards the direction of C_2H_4 generation (~78%). The endothermic nature makes such catalytic conversion a thermodynamically demanding process, and it is challenging to distinguish the rate-determining steps that govern the overall effectiveness of this catalysis under real-world conditions. Gas-phase cluster studies enable precise structural identification of active species in an unperturbed environment, and the elementary steps involved in the catalysis can be explored separately. The $Rh_xNb_y^-$ clusters are highly promising and well-defined models for probing the mechanisms of C_2H_6 and CO_2 co-conversion over condensed-phase bimetallic catalysts. Note that the realistic ODHE reaction typically operates under charge-neutral conditions over supported catalysts, while the active site that is composed of a limited number of atoms could be neutral or charged under working conditions (*e.g.*, $Pt^{\delta+}/TiO_2$ [67] and $Au^{\delta-}$–O_v–Ti^{3+} sites[68]), originating from the frequent charge transfer interaction between the active metal components and the support. In this case, clusters with a negative or positive charge can be used as active species to reveal the reaction mechanisms of related condensed-phase reactions under isolated conditions. The present calculations demonstrate that the $Rh_xNb_y^-$ clusters can mediate the ODHE of C_2H_6 to C_2H_4 at ambient conditions, while H–O coupling and H_2O desorption are kinetically and thermodynamically demanding processes and elevated temperatures are required to regenerate the cluster catalysts.

Note that the desorption of products (*e.g.*, C_2H_4, CO or H_2O) in the ODHE of C_2H_6 and CO_2 is highly composition-dependent on $Rh_xNb_y^-$ (Fig. 4A and B). Fig. 4A clearly shows that the increased number of Rh atoms in $Rh_xNb_y^-$ gradually switches the evaporation of C_2H_4 and/or H_2 from exothermic to endothermic. In the two competitive pathways, the desorption of C_2H_4 is always an enthalpy-favourable process with respect to H_2 release; thus, the two H atoms can be tightly anchored on the product $Rh_xNb_yH_2^-$ and enable the subsequent reaction with CO_2 to form H_2O. For the reaction $Rh_xNb_yH_2^- + CO_2$ (Fig. 4B), although the desorption of CO and H_2O also exhibits composition-sensitive behavior, the release of CO is consistently exothermic (ΔH_0: −1.21 to −0.76 eV), whereas H_2O escape remains thermodynamically demanding (ΔH_0: +0.18 to +1.23 eV) across all $Rh_xNb_y^-$ compositions. These results demonstrate unambiguously that the formation and desorption of H_2O is the rate-determining step to limit the overall efficiency of C_2H_6 and CO_2 co-conversion catalyzed by

Table 1 DFT-calculated barriers for C_2H_5–H cleavage, C_2H_4–H cleavage, H–H coupling, O–H coupling and H–OH coupling, as well as the absolute barriers to desorb C_2H_4, H_2, CO and H_2O in the ODHE process mediated by $Rh_xNb_y^-$ ($x + y = 5$)

Clusters	$RhNb_4^-$	$Rh_2Nb_3^-$	$Rh_3Nb_2^-$	Rh_4Nb^-
Barriers (eV)				
C_2H_5–H cleavage	+0.11	+0.44	+0.19	+0.20
C_2H_4–H cleavage	−1.14	−0.49	−0.77	+0.18
H–H coupling	−0.84	+0.16	−0.80	−0.80
O–H coupling	+0.67	+1.03	+0.86	+0.50
H–OH coupling	+2.22	+2.91	+2.09	+1.55
Absolute barriers (eV)				
C_2H_4	1.92	1.53	1.33	1.66
H_2	0.17	0.13	0.55	0.83
CO	1.93	1.58	2.07	2.55
H_2O	0.86	0.76	0.74	0.89

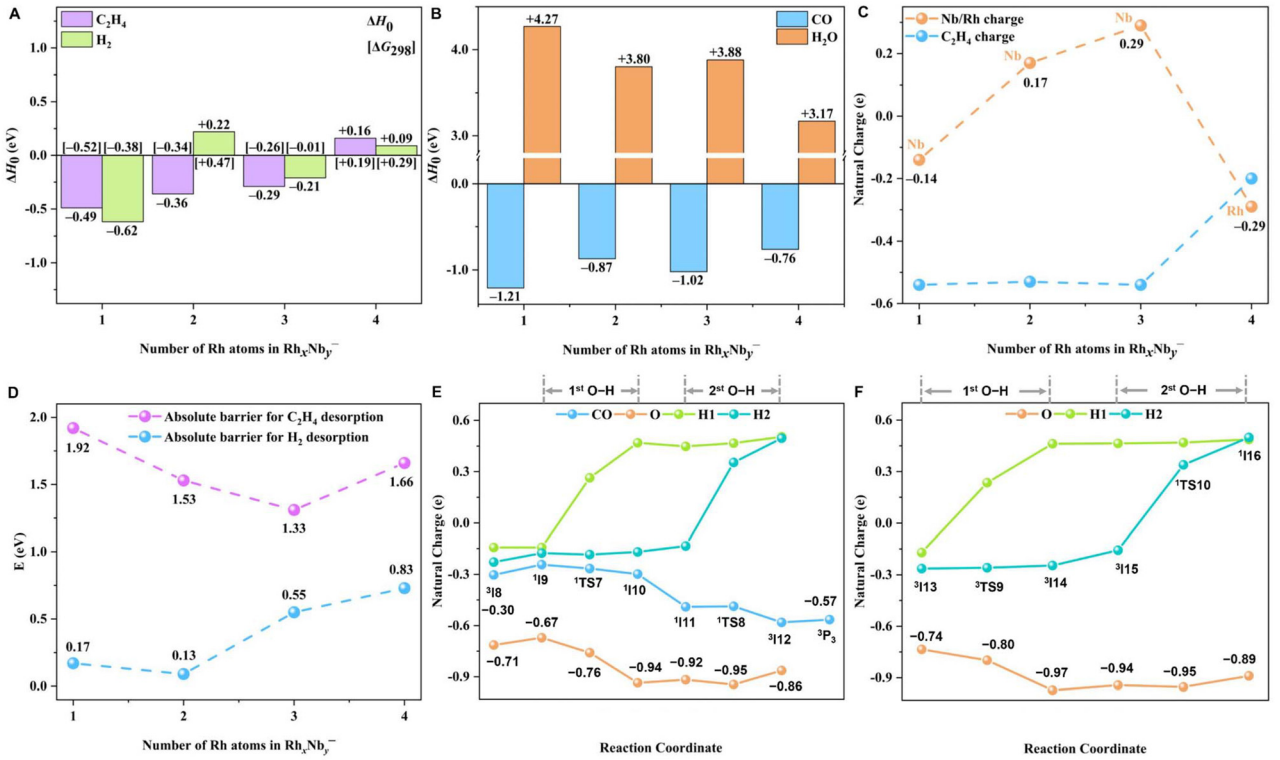

Fig. 4 Reaction heat (ΔH_0) of C_2H_4 and H_2 desorption for $Rh_xNb_y^-$ + C_2H_6 ($x + y = 5$) (A). Reaction heat (ΔH_0) of CO and H_2O desorption for $Rh_xNb_yH_2^-$ + CO_2 ($x + y = 5$) (B). Nb/Rh charge at the adsorption sites, and the charge of C_2H_4 desorption for $Rh_xNb_yC_2H_6^-$ clusters (C). DFT-calculated absolute barrier for C_2H_4 and H_2 desorption for $Rh_xNb_y^-$ + C_2H_6 ($x + y = 5$) (D). DFT-calculated natural charge (e) on the CO unit, O, H1, and H2 atoms along the pathways of CO_2 reduction mediated by $^3RhNb_4H_2^-$, [path I (E) or path II (F)].

$Rh_xNb_y^-$. Consequently, elevated temperatures are required to overcome the significant kinetic and thermodynamic barriers associated with these steps (Fig. 2 and 3 and S6–S11). The geometrical and electronic structures of crucial intermediates that govern C_2H_4 or H_2 desorption were specifically analysed to rationalize this component-sensitive behaviour. Pathway calculations on reactions $Rh_xNb_y^-$ + C_2H_6 (Fig. 2 and S6, S8, S10) demonstrated that in the intermediate before C_2H_4 desorption (*e.g.*, ^{3}I4, Fig. 2), the formed C_2H_4 molecule stands stably on a single Nb [for $Rh_xNb_y^-$ (x = 1–3) + C_2H_6] or Rh atom (for Rh_4Nb^- + C_2H_6). Thus, the charge environment of such a metal atom directly controls C_2H_4 desorption. Natural charge analysis (Fig. 4C) shows that the charged state of the Nb atom that is responsible for C_2H_4 adsorption in $Rh_xNb_y^-$ (x = 1–3) changes from negatively to positively charged with the increase in Rh atoms, while the charged state of C_2H_4 suffers from negligible perturbation, indicating the gradually strengthened Nb–C_2H_4 interaction. The negative Rh atom for the reaction Rh_4Nb^- + C_2H_6 (−0.29 e in ^{3}I90, Fig. S10) and the C_2H_4 (−0.20 e) moiety can seemingly give rise to weakened Rh–C_2H_4 bonding, while the laborious desorption of C_2H_4 can be attributed dominantly to the stronger Rh–C (6.01 eV) than the Nb–C (5.43 eV) bond.[12] This observation parallels condensed-phase experiments that Rh-containing catalysts typically induce deeper dehydrogenation of light alkanes; for example, the four C–H bonds of CH_4 tend to dissociate successively on the Rh surface because of the strong Rh–C bond.[69–71] These analyses are in reasonably good agreement with the change in thermodynamic data of C_2H_4 release (Fig. 4A). Note that the absolute barriers to desorb H_2 from the system are relatively small (0.13 eV–0.83 eV, Fig. 4D) with respect to that of C_2H_4 desorption, and the difficulty can be attributed to the substantial kinetic barriers for H_2 formation induced by the negative nature of both H adsorbates (Fig. S12).[13,72–76] Thus, the energy levels associated with H_2 escape were raised substantially and the gradual shift of the desorption site from Nb (x = 1 and 2 in $Rh_xNb_y^-$) to Rh (x = 3 and 4 in $Rh_xNb_y^-$) renders H_2 desorption energetically less favorable (Rh–H: 2.50 eV, Nb–H: 2.30 eV).[12] These extensive calculations demonstrated that the metal compositions of $Rh_xNb_y^-$ predominantly govern the reaction enthalpy of elementary steps (Fig. 4A and B) and then the ability of product (C_2H_4, H_2, CO, and H_2O) desorption from the system can be regulated accordingly. An overview of the product desorption process shows clearly that, in addition to the energy-intensive process of H_2O evaporation, C_2H_4 desorption is most sensitive to the Rh/Nb ratio in the early state of catalytic reactions (Fig. 4A and B) because the thermodynamics of C_2H_4 desorption varies gradually from an exothermic to an endothermic process. In contrast, the release of CO and H_2 from the cluster exhibits irregular fluctuations with the variation of metal composition.

To achieve high olefin selectivity and avoid over-oxidation of light alkanes into CO_x and H_2O is an important issue, especially in O_2-assisted oxidative dehydrogenation because of the highly exothermic nature of these reactions.[77] In contrast, CO_2 functions as a soft oxidant and can greatly inhibit over-oxidation and improve olefin selectivity by removing hydrogen through reverse water–gas shift.[78,79] Our predicted cluster behavior aligns with available observations on real catalysts. Condensed-phase experiments also demonstrated that a catalyst should bond the oxygen atom from CO_2 dissociation strongly enough to facilitate C–H bond cleavage and achieve high C_2H_4 selectivity.[66] Herein, the reaction of C_2H_6 with product $RhNb_4O^-$ after CO_2 reduction (Fig. S5) parallels this result that C_2H_4 can also be released readily without the formation of the intermediate CH_3CH_2O, from which the C–C scission takes place frequently.

Mechanisms of H_2O generation

An overall survey verifies that the products C_2H_4 and CO in the ODHE of C_2H_6 and CO_2 mediated by $Rh_xNb_y^-$ can be released readily under ambient conditions (Fig. 2 and 3 and S6–S11), whereas external energy is required to generate gas-phase H_2O because of the substantial kinetic barriers of O–H bond coupling and the thermodynamically demanding process of H_2O desorption. It has been frequently identified that CO adhesion on clusters can play vital roles to regulate a reaction from endothermic to exothermic and then make it a thermodynamically and kinetically more feasible process.[80–82] Herein, though CO attachment can significantly suppress the energies of crucial intermediate species during H_2O formation (Fig. 3 and S7, S9, S11), the endothermic nature of the final products (*e.g.*, $^3RhNb_4CO^-$ + H_2O, ΔH_0: +0.70 eV, Fig. 3) compared to the exothermicity of CO desorption ($^1RhNb_4OH_2^-$ + CO, ΔH_0: −1.21 eV) drives CO desorption prior to H_2O formation. Natural charge analysis reveals that the two attached H atoms carry negative charges prior to O–H coupling (Fig. 4E and F and S13), resulting in electrostatic repulsion with the oxygen atom and pronounced kinetic barriers have to be surpassed. The tight CO–Nb or CO–Rh bonding greatly stabilizes related intermediates or transition states in the pathway, while the charged states of H atoms and the oxygen atom involved in H_2O formation were negligibly perturbed (Fig. 4E and F). The leading result is that the absolute barriers of H–O coupling were only slightly affected. These results underscore that the endothermic nature of ODHE between C_2H_6 and CO_2 is primarily due to the energy required to regenerate the catalyst, namely, removing the residual H atoms and O atom, following C_2H_6 dehydrogenation and CO_2 reduction. Niobium oxide exhibits strong oxidation ability because of the existence of a unique Lewis/Brønsted acid Nb site to anchor the oxygen atom tightly.[83] Our predicted results also show clearly that after CO_2 dissociation, the leaving oxygen atom was always captured by one Nb atom (Fig. 3 and S7, S9, S11). This may be the dominant factor in making H_2O formation a challenging step of ODHE. This finding parallels the CO_2-assisted dehydrogenation of light alkanes on condensed-phase catalysts, in which the reaction endothermicity is accounted for by the subsequent reverse water–gas shift step following alkene desorption,[77,79,84] and the hydrogenation of lattice oxygen by residual H adsorbates was identified as the rate-determining step. Note that catalysts can only regulate the kinetic barriers and not disturb the reaction enthalpy. Consequently, a more evenly distributed reaction enthalpy across the elementary steps will result in a less endothermic process of the overall reaction. This finding provides an integrated and clear picture to capture the pivotal step that governs the overall efficiency of C_2H_6 and CO_2 co-conversion. Gas-phase clusters cannot fully represent the nature of active sites on heterogeneous catalysts and cannot model exactly the dynamic range of oxidation states found on realistic catalysts. Meanwhile, the well-defined oxidation states and electronic structures in gas-phase clusters are of significant importance to establish clear and molecular-level structure–activity relationships, which can serve as a foundational benchmark and a source of mechanistic hypotheses for studies of more complex and realistic systems.

Conclusion

In summary, we theoretically demonstrated that a series of $Rh_xNb_y^-$ ($x + y = 5$) clusters can mediate the oxidative dehydrogenation (ODHE) of C_2H_6 and CO_2 to give rise to C_2H_4, CO and H_2O, and composition-dependent reactivity of $Rh_xNb_y^-$ in regulating product desorption was identified. It was found that desorption of products C_2H_4 and CO occurs under ambient conditions, and the increased number of Rh atoms in $Rh_xNb_y^-$ results in enhanced barriers for C_2H_4 desorption. The reasons behind this selective desorption of C_2H_4 from C_2H_6 rather than CH_4 or H_2 were rationalized. Meanwhile, the final formation and escape of H_2O to regenerate $Rh_xNb_y^-$ catalysts represent the rate-determining steps that govern the overall efficiency of ODHE. This finding decouples the individual elemental steps from the complex catalytic process of C_2H_6 and CO_2 co-conversion and identifies unanimously the energetically demanding step of H_2O generation that leads to the highly endothermic nature of this ODHE.

Author contributions

H. Z. performed the theoretical calculations and organized the raw data. H. Z. and X.-Y. S. analyzed the calculation results. H. Z. and X.-N. L. wrote the manuscript. ORCID: https://orcid.org/0000-0002-0316-5762.

Conflicts of interest

The authors declare no competing financial interest.

Data availability

The data supporting this article have been included as part of the supplementary information (SI). Supplementary information is available. Details of additional theoretical results (DFT-calculated structures and reaction mechanisms, and natural charge analysis). See DOI: https://doi.org/10.1039/d5dt02594j.

Acknowledgements

This work was financially supported by the National Key R&D Program of China (2021YFA1500704) and the National Natural Science Foundation of China (22473012 and 92461313).

References

1 M. Filonchyk, M. P. Peterson, H. Yan, A. Gusev, L. Zhang, Y. He and S. Yang, *Sci. Total Environ.*, 2024, **944**, 173895.
2 M. Filonchyk, M. P. Peterson, L. Zhang, V. Hurynovich and Y. He, *Sci. Total Environ.*, 2024, **935**, 173359.
3 W. F. Lamb, T. Wiedmann, J. Pongratz, R. Andrew, M. Crippa, J. G. J. Olivier, D. Wiedenhofer, G. Mattioli, A. Al Khourdajie, J. House, *et al.*, *Environ. Res. Lett.*, 2022, **17**, 049502.
4 M. M. Rahman, K. Alam and E. Velayutham, *Energy Rep.*, 2022, **8**, 2793–2805.
5 T. Liang, L. Chai, J. Tan, Y. Jing and L. Lv, *Appl. Energy*, 2024, **367**, 123390.
6 M. Loipersberger, D. Z. Zee, J. A. Panetier, C. J. Chang and J. R. Long, *Inorg. Chem.*, 2020, **59**, 8146–8160.
7 S. Valluri, V. Claremboux and S. Kawatra, *J. Environ. Sci.*, 2022, **113**, 322–344.
8 L. Calzadiaz-Ramirez and A. S. Meyer, *Curr. Opin. Biotechnol.*, 2022, **73**, 95–100.
9 J. Kim, A. Seong, Y. Yang, S. Joo, C. Kim, D. H. Jeon, L. Dai and G. Kim, *Nano Energy*, 2021, **82**, 105741.
10 C. Chen, X. Feng, Q. Zhu, R. Dong, R. Yang, Y. Cheng and C. He, *Inorg. Chem.*, 2019, **58**, 2717–2728.
11 Z. Ye, L. Liu, X. Luo, P. Gao, T. Wu and S. Sun, *Inorg. Chem.*, 2025, **64**, 519–529.
12 Y.-R. Luo, *Comprehensive Handbook of Chemical Bond Energies*, CRC Press, 2007.
13 J.-J. Chen, X.-N. Li, Q.-Y. Liu, G.-P. Wei, Y. Yang, Z.-Y. Li and S.-G. He, *J. Phys. Chem. Lett.*, 2021, **12**, 8513–8520.
14 L. A. Davis, *Engineering*, 2018, **4**, 438–439.
15 T. Zhang, Z.-C. Liu and W.-M. Yang, *Sci. China: Chem.*, 2021, **51**, 154–164.
16 Z. Ma, G. Pi, X. Dong and C. Chen, *Renewable Sustainable Energy Rev.*, 2017, **67**, 1300–1307.
17 Z. Xie, D. Tian, M. Xie, S.-Z. Yang, Y. Xu, N. Rui, J. H. Lee, S. D. Senanayake, K. Li and H. Wang, *Chem*, 2020, **6**, 2703–2716.
18 B. Liu, S. Babaei, L. Bai, S. Tian, H. Ghasemzadeh, M. Rashidi and M. Ostadhassan, *Chem. Eng. J.*, 2022, **450**, 138242.
19 J. Li, P. Li, S. Zhou, Z. Sun, B. Meng and Y. Li, *Chem. Eng. J.*, 2022, **444**, 136617.
20 X. Shi, S. Ji and K. Wang, *Catal. Lett.*, 2008, **125**, 331–339.
21 B. Yan, S. Yao, S. Kattel, Q. Wu, Z. Xie, E. Gomez, P. Liu, D. Su and J. G. Chen, *Proc. Natl. Acad. Sci. U. S. A.*, 2018, **115**, 8278–8283.
22 M. D. Porosoff, M. N. Z. Myint, S. Kattel, Z. Xie, E. Gomez, P. Liu and J.-G. Chen, *Angew. Chem., Int. Ed.*, 2015, **54**, 15501–15505.
23 M. Myint, B. Yan, J. Wan, S. Zhao and J.-G. Chen, *J. Catal.*, 2016, **343**, 168–177.
24 W. M. Haynes, *CRC Handbook of Chemistry and Physics*, CRC Press, 2014.
25 S. Yao, B. Yan, Z. Jiang, Z. Liu, Q. Wu, J. H. Lee and J.-G. Chen, *ACS Catal.*, 2018, **8**, 5374–5381.
26 B. Yan, S. Yao and J.-G. Chen, *ChemCatChem*, 2020, **12**, 494–503.
27 Z. Xie, B. Yan, J. H. Lee, Q. Wu, X. Li, B. Zhao, D. Su, L. Zhang and J. G. Chen, *Appl. Catal., B*, 2019, **245**, 376–388.
28 Q. Liu, J. Ma and C. Chen, *Chin. J. Catal.*, 2022, **43**, 898–912.
29 X.-N. Li, X.-P. Zou and S.-G. He, *Chin. J. Catal.*, 2017, **38**, 1515–1527.
30 L. Liu and A. Corma, *Chem. Rev.*, 2018, **118**, 4981–5079.
31 H. Schwarz and K. R. Asmis, *Chem. – Eur. J.*, 2019, **25**, 2112–2126.
32 H. Schwarz, *Catal. Sci. Technol.*, 2017, **7**, 4302–4314.
33 D. J. Harding and A. Fielicke, *Chem. – Eur. J.*, 2014, **20**, 3258–3267.
34 S. M. Lang and T. M. Bernhardt, *Phys. Chem. Chem. Phys.*, 2012, **14**, 9255–9269.
35 X.-N. Li, L.-N. Wang, L.-H. Mou and S.-G. He, *J. Phys. Chem. A*, 2019, **123**, 9257–9267.
36 W. Gan, B. Huang, C. Cui, K. Hansen and Z. Luo, *ChemPhysChem*, 2023, **24**, e202200530.
37 Y. Jia, L. Geng, H. Zhang and Z. Luo, *ChemistrySelect*, 2022, **7**, e202203632.
38 Y.-H. Zhang and J.-B. Ma, *J. Phys. Chem. A*, 2024, **128**, 2323–2329.
39 H.-Y. Zhou, M. Wang, Y.-Q. Ding and J.-B. Ma, *Dalton Trans.*, 2020, **49**, 14081–14087.
40 X.-Y. He, Y.-Z. Liu, S.-D. Wang, X. Lan, X.-N. Li and S.-G. He, *Dalton Trans.*, 2022, **51**, 11491–11498.
41 Y.-X. Zhao, B. Yang, H.-F. Li, Y. Zhang, Y. Yang, Q.-Y. Liu, H.-G. Xu, W.-J. Zheng and S.-G. He, *Angew. Chem., Int. Ed.*, 2020, **59**, 21216–21223.
42 Y. Yang, Y.-K. Li, Y.-X. Zhao, G.-P. Wei, Y. Ren, K. R. Asmis and S.-G. He, *Angew. Chem., Int. Ed.*, 2021, **60**, 13788–13792.
43 A. Zhao, Q.-Y. Liu, Z.-Y. Li, X.-N. Li and S.-G. He, *Dalton Trans.*, 2024, **53**, 8347–8355.
44 Y.-Z. Liu, X.-Y. He, J.-J. Chen, Z.-P. Zhao, X.-N. Li and S.-G. He, *Dalton Trans.*, 2023, **52**, 6668–6676.

45 Y. Gao, Z. Cai, X. Wu, Z. Lv, P. Wu and C. Cai, *ACS Catal.*, 2018, **8**, 10364–10374.
46 L. Zhang, Z. Huang, D. Zhang and S. Xia, *Inorg. Chem.*, 2025, **64**, 15448–15462.
47 M.-Q. Zhang, Y.-X. Zhao and S.-G. He, *Chem. Bull.*, 2016, **79**, 395–402.
48 M. Lein, *Coord. Chem. Rev.*, 2009, **253**, 625–634.
49 N. Berkaïne, P. Reinhardt and M. E. Alikhani, *Chem. Phys.*, 2008, **343**, 241–249.
50 K. M. Altus and J. A. Love, *Commun. Chem.*, 2021, **4**, 173.
51 H. Zhou, M. Ruan, Q.-Y. Liu, Y.-X. Zhao, R.-Y. Wang, Y. Yang and S.-G. He, *Phys. Chem. Chem. Phys.*, 2024, **26**, 14186–14193.
52 R. Colombo, G. Moroni, C. Negri, G. Delen, M. Monai, A. Donazzi, B. M. Weckhuysen and M. Maestri, *Angew. Chem., Int. Ed.*, 2024, **63**, e202408668.
53 Y. Zhang and G.-C. Wang, *J. Phys. Chem. C*, 2021, **125**, 26530–26541.
54 Y. Yang, B. Yang, Y.-X. Zhao, L.-X. Jiang, Z.-Y. Li, Y. Ren, H.-G. Xu, W.-J. Zheng and S.-G. He, *Angew. Chem., Int. Ed.*, 2019, **58**, 17287–17292.
55 Y. Yang, L.-J. Zhang, X.-L. Wang, R. Wang, Y.-X. Zhao, S.-G. He and S.-Q. Zang, *J. Am. Chem. Soc.*, 2025, **147**, 362–371.
56 A. Zhao, Y.-X. Zhao, Q. Li, X.-G. Zhao, Q.-Y. Liu and S.-G. He, *Angew. Chem., Int. Ed.*, 2025, **64**, e202503132.
57 B. Yan, X. Yang, S. Yao, J. Wan, M. Myint, E. Gomez, Z. Xie, S. Kattel, W. Xu and J. G. Chen, *ACS Catal.*, 2016, **6**, 7283–7292.
58 X. Chen, S. Li, Z. Xu, H. Li, J. Li, Y. Fu and J. Zhang, *Int. J. Hydrogen Energy*, 2025, **103**, 501–512.
59 X. Zhang, Q. Ye, B. Xu and D. He, *Catal. Lett.*, 2007, **117**, 140–145.
60 R. Koirala, R. Buechel, S. E. Pratsinis and A. Baiker, *Appl. Catal., A*, 2016, **527**, 96–108.
61 Z. Shen, J. Liu, H. Xu, Y. Yue, W. Hua and W. Shen, *Appl. Catal., A*, 2009, **356**, 148–153.
62 R. Koirala, R. Buechel, F. Krumeich, S. E. Pratsinis and A. Baiker, *ACS Catal.*, 2015, **5**, 690–702.
63 E. Asghari, M. Haghighi and F. Rahmani, *J. Mol. Catal. A: Chem.*, 2016, **418–419**, 115–124.
64 N. Mimura, I. Takahara, M. Inaba, M. Okamoto and K. Murata, *Catal. Commun.*, 2002, **3**, 257–262.
65 N. Mimura, M. Okamoto, H. Yamashita, S. T. Oyama and K. Murata, *J. Phys. Chem. B*, 2006, **110**, 21764–21770.
66 Z. Xie, X. Wang, X. Chen, P. Liu and J. G. Chen, *J. Am. Chem. Soc.*, 2022, **144**, 4186–4195.
67 S. C. Ammal and A. Heyden, *ACS Catal.*, 2017, **7**, 301–309.
68 N. Liu, M. Xu, Y. Yang, S. Zhang, J. Zhang, W. Wang, L. Zheng, S. Hong and M. Wei, *ACS Catal.*, 2019, **9**, 2707–2717.
69 M. A. A. Aziz, H. D. Setiabudi, L. P. Teh, N. H. R. Annuar and A. A. Jalil, *J. Taiwan Inst. Chem. Eng.*, 2019, **101**, 139–158.
70 H. Wu, X.-N. Wu, X. Jin, Y. Zhou, W. Li, C. Ji and M. Zhou, *JACS Au*, 2021, **1**, 1631–1638.
71 R. Tsuchida, H. Kurokawa, T. Yamamoto and H. Ogihara, *ChemCatChem*, 2025, **17**, e202401386.
72 L.-S. Chen, Y.-Z. Liu, J.-J. Chen, S.-D. Wang, T.-M. Ma, X.-N. Li and S.-G. He, *J. Phys. Chem. A*, 2022, **126**, 5294–5301.
73 H. Zhang, M. Zhang, Y. Jia, L. Geng, B. Yin, S. Li, Z. Luo and F. Pan, *J. Phys. Chem. Lett.*, 2021, **12**, 1593–1600.
74 J.-X. Liang, J. Lin, J. Liu, X. Wang, T. Zhang and J. Li, *Angew. Chem., Int. Ed.*, 2020, **59**, 12868–12875.
75 H. Zhang, H. Wu, Y. Jia, B. Yin, L. Geng, Z. Luo and K. Hansen, *Commun. Chem.*, 2020, **3**, 148.
76 R. O. Ramabhadran, J. E. Mann, S. E. Waller, D. W. Rothgeb, C. C. Jarrold and K. Raghavachari, *J. Am. Chem. Soc.*, 2013, **135**, 17039–17051.
77 Y. Zheng, X. Zhang, J. Li, J. An, L. Xu, X. Li and X. Zhu, *Chin. J. Catal.*, 2024, **65**, 40–69.
78 S. Najari, S. Saeidi, P. Concepcion, D. D. Dionysiou, S. K. Bhargava, A. F. Lee and K. Wilson, *Chem. Soc. Rev.*, 2021, **50**, 4564–4605.
79 S. Zhang, C. Wu, J. Xin, G. Yang, Y. Li, M. Su, H. Zhang, H. Zhang and L. Wang, *ChemPhysChem*, 2025, **26**, e202401073.
80 X.-P. Zou, L.-N. Wang, X.-N. Li, Q.-Y. Liu, Y.-X. Zhao, T.-M. Ma and S.-G. He, *Angew. Chem., Int. Ed.*, 2018, **57**, 10989–10993.
81 L.-N. Wang, X.-N. Li and S.-G. He, *J. Phys. Chem. Lett.*, 2019, **10**, 1133–1138.
82 L.-S. Chen, J.-J. Chen, T.-M. Ma, X.-N. Li and S.-G. He, *Chem. Phys. Lett.*, 2022, **787**, 139276.
83 K. Su, H. Liu, Z. Gao, P. Fornasiero and F. Wang, *Adv. Sci.*, 2021, **8**, 2003156.
84 C. Chu, B. Chen, Y. He, G. Jiang, X. Lan, S. Li, C. Wu and D. Cao, *ACS Catal.*, 2024, **14**, 9662–9677.

